Indoor Through-the-wall Passive Human Target Detection With WiFi

YANG Xiaolong* , Member, IEEE , WU Shiming* , ZHOU Mu* , Senior Member, IEEE,
XIE Liangbo* , Member, IEEE, WANG Jiacheng* , HE Wei*
*School of Communication and Information Engineering, Chongqing University of Posts and Telecommunications
Email: {yangxiaolong, zhoumu, xieliangbo, hewei}@cqupt.edu.cn, {wu_shiming, jcwang_cq}@foxmail.com

***Abstract*—Passive human target detection has a broad application prospect in security monitoring, intelligent home and human-computer interaction. In through-the-wall scenario, due to the serious attenuation of signals caused by wall, the energy of target reflection signal decreases significantly and is submerged in the direct signal of the transceiver and the reflection signal of indoor static objects, making it difficult to be extracted. Therefore, the existing WiFi sensing system has some limitations in through-the-wall scene, especially in detection of the stationary human target and the number of moving human targets. According to the above problem, we propose a detection system TWMD based on multidimensional signal features in this paper. Firstly, the received Channel State Information (CSI) data is preprocessed to eliminate the phase error and amplitude noise. Then, the multidimensional features are fully extracted from the correlation coefficient matrix by using time correlation and subcarrier correlation of CSI. Finally, the mapping between features and detection results is established by Back Propagation (BP) neural network. Our experimental results show that the recognition accuracy of TWMD in the environment with glass wall, brick wall and concrete wall are above 0.980, 0.900, 0.850, respectively. Compared with the existing detection system based on single signal feature, it improves about 0.450 in the detection of the number of moving targets.**

***Index Terms*—Passive human target detection, WiFi, channel state information, multidimensional signal features**

I. Introduction

Unlike active target detection technology, which requires specialized hardware attached to the target, passive target detection technology means the target need not to carry any device. It is not only widely used in hospitals, nursing homes, museums, archives and other places that need monitoring the status of personnel [1], but also the basis of realizing intelligent home [2,3] and human-computer interaction [4]. Traditional passive human target detection is accomplished by infrared ray, camera and other photoelectric equipment[5]. In recent years, as WiFi devices have been widely deployed in various locations, some researchers try to use WiFi signal for environment sensing. The research of WiFi based target detection revolves around Received Signal Strength Indication (RSSI) and Channel State Information (CSI). RSSI based solution is mainly detected by capturing RSSI jitter caused by human interference [6]. Since RSSI is only a description of the received power, there are problems such as coarse grained detection and vulnerability to environmental noise, especially when the target has little impact on the environment, it is prone to false detection. Different from RSSI, the CSI contains both amplitude and phase information for each propagation path with a finer granularity of detection.

CSI based indoor human target detection can be divided into two scenarios, line of sight (LoS) which means the transmitter and receiver are in one room, and through-the-wall which means the transmitter and receiver are located on both sides of the wall. Currently, most works focus on LoS scenario. In [7], static and dynamic signal modes are distinguished by the maximum eigenvalue of signal correlation matrix to detect the moving target. In [8], the percentage of non-zero elements in the CSI matrix is chosen as the feature, and a monotone function between the number of target and the feature is established to achieve target counting. PADS [9] and DeMan [10] recognize whether there is a moving human target by evaluating the stability of CSI amplitude and phase. In [11], the human target detection scheme based on fingerprint database and threshold is designed by utilizing the indoor multipath effect.

However, the passive human target detection in the through-the-wall scenario is still an open issue. The difficulty is that the wireless signal has a serious attenuation when it passes through the wall, and the target reflection signal is submerged in the direct path signal of transceiver and the reflected signal of static objects, which increases the difficulty of signal analysis. In [12], a MIMO system is built on USRP to detect moving targets behind the wall and even track the target motion trajectory. However, this system is hard to detect static human target, and it relies on a non-commercial WiFi platform and an expensive external clock. In [13], by calculating the average Doppler spectrum of CSI, two features are calculated for detection, but this system is not ideal in distinguishing the number of human targets. In [14], a detection system R-TTWD is designed by analyzing the correlation of different subcarriers, however, due to the single feature dimension and quantity, the detection of the number of moving human targets is limited. According to the above problems, we design a novel detection system TWMD based on commercial WiFi equipment. Different from

The Scientific and Technological Research Foundation of Chongqing Municipal Education Commission (KJQN201800625), The National Natural Science Foundation of China (No.61771083, N0.61704015), Program for Changjiang Scholars and Innovative Research Team in University (No.IRT1299)

978-1-7281-0960-2/19/$31.00 ©2019 IEEE

the previous detection scheme utilizing single feature, a new detection idea that expands the dimension and quantity of features and then builds Back Propagation (BP) neural network to obtain the mapping relationship between multiple features and detection results is proposed in TWMD. This detection scheme can avoids the system instability caused by improper feature selection and insufficient number of features. At the same time, in order to enhance the reliability of TWMD in low SNR environments, the output features of BP neural network of each antenna are merged. In summary, our main contributions are as follows.

- A design for indoor through-the-wall passive human target detection system TWMD using commodity WiFi devices is proposed in our work. Different from the previous single feature based detection scheme, TTWD is a multidimensional features based detection system, which extracts features from the correlation coefficient matrix by using CSI timing correlation and subcarrier correlation, and BP neural network with stronger mapping ability is used to complete the mapping between the features and the detection results. To the best of our knowledge, TTWD is the first system which can detect the stationary human target and the number of moving human targets in through-the-wall scenarios.
- We propose a method that merges the output features of each antenna of the MIMO system we build to enable more accurate and robust detection.
- We validate the performance of TWMD in different indoor environment. Our experimental results show that the recognition accuracy in the environment with glass wall, brick wall and concrete wall is above 0.980, 0.900, 0.850, respectively. Especially, compared with the existing detection algorithm based on single signal feature, it improves about 0.450 in the detection of the number of moving targets.

The remaining chapters are organized as follows. The system framework of TWMD is introduced in Section 2 and then we describe the multidimensional signal feature extraction and detection in detail in Section 3. In Section 4, we validate the performance of TWMD and discuss the influence of various variables on detection results fully. At last, we summarize this paper and look forward to further work in Section 5.

II. Overview of System

TTWD consists of one transmitter and one receiver, and this two machines are placed on both sides of the wall. The system architecture is shown in Fig.1, including: 1) Data preprocessing: we perform a linear transformation for CSI phase to obtain the calibrated phase firstly. Then the outliers of CSI data are removed, and reconstructed by linear interpolation. At last, the amplitude noise is removed by the wavelet threshold denoising. 2) Multidimensional feature extraction: we calculate the amplitude correlation coefficient matrix and phase correlation coefficient matrix of CSI data in a time window and extract the first two major eigenvalues of the matrix as time domain features. Then we calculate the subcarrier correlation

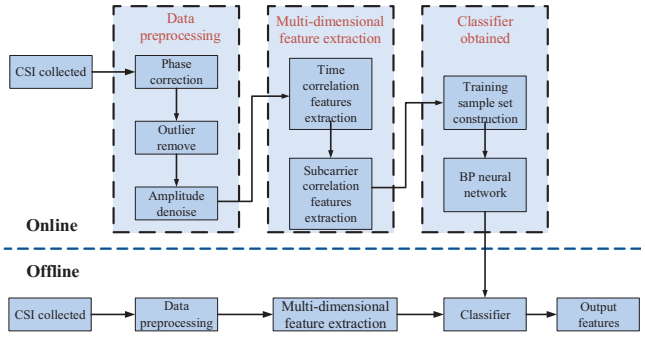

Fig. 1. System architecture of TWMD.

coefficient matrix, and extract subcarrier domain features by the eigenvector and principal components of it. 3) Classifier obtained: the training sample set is constructed according to the extracted features, and put into BP neural network for training to obtain a classifier for realtime detection online.

III. METHODOLOGY

A. Data preprocessing

CSI refers to the channel impulse response, which can reflect the channel characteristics such as multipath effect, shadow fading, and distortion of the received signal. TWMD implements IEEE 802.11n protocol and adopts OFDM modulation. Suppose there are M packets in a time window, the extracted CSI from one receive antenna can be represented as a receiving matrix:

$$\mathbf{H} = \begin{bmatrix} h_{1,1} & h_{1,2} & \cdots & h_{1,M} \\ \vdots & \vdots & \ddots & \vdots \\ h_{K,1} & h_{K,2} & \cdots & h_{K,M} \end{bmatrix} \tag{1}$$

where K represents the total number of subcarriers and $h_{k,m}$ represents the sum of the impulse responses of all propagation paths on the k^{th} subcarrier of the m^{th} packet, which can be expressed as

$$h_{k,m} = \|h_{k,m}\| e^{-j\angle h_{k,m}} = \sum_{l=1}^{L} \alpha_{k,m}^{l} e^{-j2\pi f_k \tau_{k,m}^{l}} \tag{2}$$

where $\|h_{k,m}\|$ and $\angle h_{k,m}$ represent the amplitude and phase of $h_{k,m}$, respectly. L is the total number of signal propagation paths, f_k is the frequency of the k^{th} subcarrier. $\alpha_{k,m}^{l}$ and $\tau_{k,m}^{l}$ represent the amplitude attenuation coefficient and propagation delay of the l^{th} path, respectively.

Out-synchronization of transceiver and insufficient hardware accuracy can cause carrier frequency offset, sampling frequency offset, etc. Within a certain range, these errors do not degrade the quality of the communication, but have a large impact on the CSI phase. The phase of the received CSI can be expressed as:

$$\hat{\theta}_k = \theta_k + \frac{2\pi}{K} k\varphi + \varepsilon \tag{3}$$

where $\hat{\theta}_k$ and θ_k represent the measured phase and the true phase of the k^{th} subcarrier, respectively, φ is the phase offset, and ε is the constant phase deviation. In our work, a linear

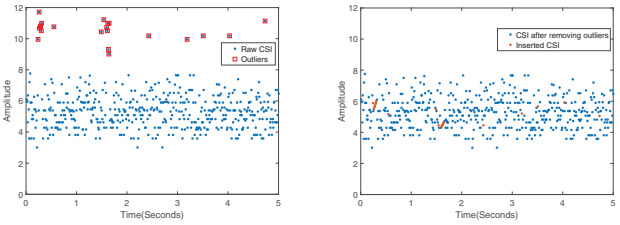

(a) Outlier detection (b) Delete outliers and interpolate

Fig. 2. Outlier remove

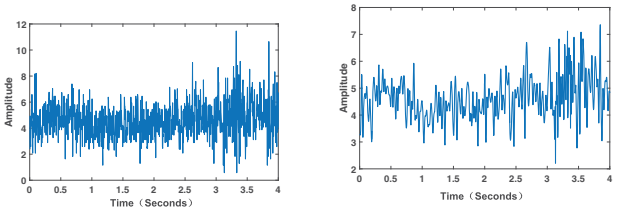

(a) Before denoising (b) After denoising

Fig. 3. Comparison before and after wavelet threshold denoising

transformation is performed for CSI phase to eliminate the phase error [15]. Assume that the subcarrier number is an increasing sequence $\{k_j\}_{j=1}^{n}$, and the processed phase is:

$$\tilde{\theta}_{k_j} = \theta_{k_j} - \frac{k_j}{k_n - k_1}(\theta_{k_n} - \theta_{k_1}) - \frac{1}{n}\sum_{i=1}^{n}\theta_{k_i} \quad (4)$$

Where $\tilde{\theta}_{k_j}$ and θ_{k_j} represent the measured phase and true phase of the subcarrier which the number is k_j, respectively. What we are interested in is the trend of the phase, not the true phase value. This linear phase transformation does not change the trend of the phase, thus meeting the subsequent requirements.

The CSI amplitude preprocessing includes two parts: outlier removal and wavelet threshold denoising. There are always some outliers away from the overall sample for CSI data received over a continuous period of time, as shown by the dots in the red box in Fig.2(a). These outliers are caused by the contingency factors of the transceiver system or the environment and can not represent the real channel state. In order to eliminate the interference of the outliers, we remove the points other than $[\mu - \eta \times \sigma, \mu + \eta \times \sigma]$, where μ is the median of a set of observations, σ is the absolute deviation of the median, and η is the empirical constant which equals 3 in our work. After removing the outliers, the new data is inserted by linear interpolation method at the vacancy, as shown in Fig.2(b).

The wavelet threshold method is further used to denoise the amplitude after eliminating the influence of outliers [16]. We choose Gaussian function as wavelet base to decompose the signal in 5 layers and soft threshold method to process the detail coefficients. As shown in Fig.3, The amplitude has a lot of burrs before denoising while the denoised waveform is smooth which can better reflect the channel change trend.

B. Multi-dimensional feature extraction

Channel is relatively stable when there is no one in the detected area, while it be unstable when there is a moving human or a stationary human who does light exercise (such as writing, drinking, etc.). The stability of channel is reflected in two aspects: 1) the amplitude and phase of each subcarrier as a function of time; 2) the correlation between different subcarriers over a period of time. By capturing the influence of human body on channel, it can be judged whether there is no one in the room or not. Further, the number of moving targets can be detected based on the degree of influence on the channel. Therefore, how to obtain comprehensive and effective features has an important impact on detection results. Different from the previous detection schemes utilizing single feature, in order to achieve more fine-grained detection, the multidimensional features are fully extracted from time domain correlation and subcarrier correlation.

Equation (1) can be expressed as follows after data processing:

$$\tilde{\mathbf{H}} = \begin{bmatrix} \tilde{h}_{1,1} & \tilde{h}_{1,2} & \cdots & \tilde{h}_{1,M} \\ \vdots & \vdots & \ddots & \vdots \\ \tilde{h}_{K,1} & \tilde{h}_{K,2} & \cdots & \tilde{h}_{K,M} \end{bmatrix} \quad (5)$$

let $\mathbf{g_m} = [\tilde{h}_{1,m}, \tilde{h}_{2,m}, \cdots, \tilde{h}_{K,m}]^T$ denote the CSI of all subcarriers in the m^{th} packet, and $\mathbf{r_k} = [\tilde{h}_{k,1}, \tilde{h}_{k,2}, \cdots, \tilde{h}_{k,M}]^T$ denote the CSI of the k^{th} subcarrier in a time window. The CSI amplitude correlation coefficient $a_{m,n}$ of the m^{th} packet and the n^{th} packet is calculated as follows:

$$\begin{aligned} a_{m,n} &= corr(\|\mathbf{g_m}\|, \|\mathbf{g_n}\|) \\ &= \frac{1}{K}\sum_{k=1}^{K}\left(\frac{\left\|\tilde{h}_{k,m}\right\| - \mu_m}{\sigma_m}\right)\left(\frac{\left\|\tilde{h}_{k,n}\right\| - \mu_n}{\sigma_n}\right) \end{aligned} \quad (6)$$

where

$$\begin{cases} \mu_m = \frac{1}{K}\sum\limits_{k=1}^{K}\tilde{h}_{k,m} \\ \mu_n = \frac{1}{K}\sum\limits_{k=1}^{K}\tilde{h}_{k,n} \\ \sigma_m = \sqrt{\frac{1}{K}\sum\limits_{k=1}^{K}\left(\tilde{h}_{k,m} - \mu_m\right)^2} \\ \sigma_n = \sqrt{\frac{1}{K}\sum\limits_{k=1}^{K}\left(\tilde{h}_{k,n} - \mu_n\right)^2} \end{cases} \quad (7)$$

The greater the correlation is, the larger the correlation coefficient is. The CSI amplitude time domain correlation coefficient matrix can be calculated as $\mathbf{A} = (a_{m,n})_{M\times M}$, which is a real symmetric matrix. Similarly, the phase time domain correlation coefficient matrix $\mathbf{C} = (c_{m,n})_{M\times M}$, where $c_{m,n}$ can be calculated as follow:

$$c_{m,n} = corr(\angle\mathbf{g_m}, \angle\mathbf{g_n}) \quad (8)$$

we perform eigen-decomposition of matrix $\mathbf{A}$ and $\mathbf{C}$,and sort the eigenvalues in descending order, as:

$$\mathbf{\Lambda} = [\lambda_1, \lambda_2, \cdots, \lambda_M], (\lambda_i < \lambda_{i+1}, i \in [1, M-1]) \quad (9)$$

$$\mathbf{\Gamma} = [\gamma_1, \gamma_2, \cdots, \gamma_M], (\lambda_i < \lambda_{i+1}, i \in [1, M-1]) \quad (10)$$

the main information of matrix $\mathbf{A}$ and $\mathbf{C}$ is in the first and second eigenvalues which are more greater than others,

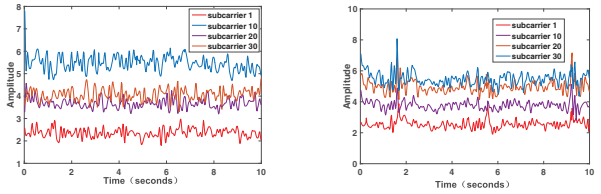

(a) Human-free (b) Human presence

Fig. 4. Correlation of subcarriers for human-free and human presence

therefore, λ_1 , λ_2 , γ_1 and γ_2 are selected as time domain correlation features.

Figure 4 shows the fluctuations in CSI amplitude over time for the 1th, 10th, 20th, and 30th subcarriers. Obviously, when no human in the scenario, the waveform fluctuation trend of different subcarriers is independent, that is, the correlation is small, and when there is a human, the waveforms of different subcarriers show similar trends, and the correlation is greater. Based on the analysis above, the subcarrier correlation coefficient of the m^{th} subcarrier and the n^{th} subcarrier is calculated as:

$$s_{m,n} = corr(\|\mathbf{r_m}\|, \|\mathbf{r_n}\|) \tag{11}$$

and the matrix $\mathbf{S} = (s_{m,n})_{K\times K}$ represents the subcarrier correlation coefficient matrix. We extract features from the principal components and eigenvectors of matrix $\mathbf{S}$. After eigen-decomposition is performed on matrix $\mathbf{S}$, the eigenvalues are arranged in descending order, and the corresponding eigenvector is $\mathbf{e}_1$,$\mathbf{e}_2$,$\cdots$,$\mathbf{e}_K$. The first order difference mean of the eigenvectors is calculated as:

$$\phi_i = \frac{1}{K-1}\sum_{k=2}^{K} |\mathbf{e}_i(k) - \mathbf{e}_i(k-1)| \tag{12}$$

Literature [14] considers that $\mathbf{e}_1$ contains noise and only extracts ϕ_2 and ϕ_3 as signal characteristics. However, we find that after data preprocessing, the useful signal in $\mathbf{e}_1$ is larger than the noise information. In order to avoid the loss of useful information, we takes ϕ_1, ϕ_2, and ϕ_3 as features. In addition, the magnitude distribution of $\tilde{\mathbf{H}}$ is normalized, denoted as $\mathbf{Z}$, and $\mathbf{Z}$ is projected into the vector space corresponding to the feature vector to obtain the respective principal components:

$$\mathbf{p_i} = \mathbf{Z} \times \mathbf{e}_i \tag{13}$$

We calculate the variance of $\mathbf{p_i}$, denoted as β_i , and take β_1 , β_2 , β_3 as features. The sample space $\mathbf{F} = [\lambda_1, \lambda_2, \gamma_1, \gamma_2, \beta_1, \beta_2, \beta_3, \phi_1, \phi_2, \phi_3]$ can be constructed based on the features extracted from the time correlation coefficient matrix and the subcarrier correlation coefficient matrix above.

C. Classifier construction

BP neural network with stronger mapping ability is selected to complete classification [17]. The input features is $\mathbf{F}$, the number of hidden layer neurons is 10, and the excitation function is sigmod function. Output features is $\mathbf{F}' = [\Omega_1, \Omega_2, \Omega_3, \Omega_4]$, where Ω_1 ,...,Ω_4 , represent no human target, one moving or stationary human target, two moving human targets, and three moving human targets, respectively. In addition, three receiving antennas are used to enhance the robustness of TWMD. After obtaining the output features of three receiving antennas denoted as $\mathbf{F'}_1$, $\mathbf{F'}_2$, $\mathbf{F'}_3$, the final output feature is $\mathbf{F''} = \mathbf{F'}_1 + \mathbf{F'}_2 + \mathbf{F'}_3$.

Fig. 5. Experimental data collection

IV. EXPERIMENTS AND EVALUATION

A. Experimental methodology

We use two minicomputers equipped with Intel 5300 wireless network card and CSI kit as the transmitter and the receiver. The transmitter is equipped with a directional antenna and the receiver is equipped with three TP-Link omnidirectional antennas. Figure 5 shows that the transceivers are placed on both sides of the wall for data transmission, while a volunteer walks randomly in the room. Our experiments are conducted in three typical office environment: glass walls, brick walls, and concrete walls. In addition, we divide the detected room into four areas A, B, C, and D, as shown in Fig.6.

The data collected in each experimental scenario includes the following categories: 1) no one in the room; 2) one people walking randomly in the A, B, C, and D areas, or a stationary people stretching; 3) two people walking randomly in the A, B, C, and D areas; 4) three people walking randomly in the A, B, C, and D areas. By this way, it can be considered that each category of experimental data cover all areas of detected room. In addition, the volunteers are composed of 4 different body types and different ages, avoiding the influence of the body shape and gait of the volunteers on the experimental results.

B. Feature analysis

In order to analyze the performance of selected signal features, we normalize each feature, observe its cumulative distribution function and analyze them. Taking the brick wall experimental scenario as an example, Fig.7 shows the cumulative distribution function graph for each feature. The cumulative distribution function of each feature has a large overlap, and it is difficult to find a suitable threshold for detection if only one or two signal features are used. For example, λ_1 and γ_1 are used as features in DeMan [10], and the detection effect is shown in Fig.8(a). All the feature points are mixed and difficult to distinguish. ϕ_2 and ϕ_3 are used as features in R-TTWD [14], and the detection effect is shown in Fig.8(b). This detection scheme can distinguish between unmanned (red dots) and moving people (points other than red), but the different numbers of moving targets are hard to be distinguished.

C. Detection cycle analysis

The performance indicator for a multi-classification system relies on the detection accuracy of each category which refers to the ratio of the number of samples that a category is

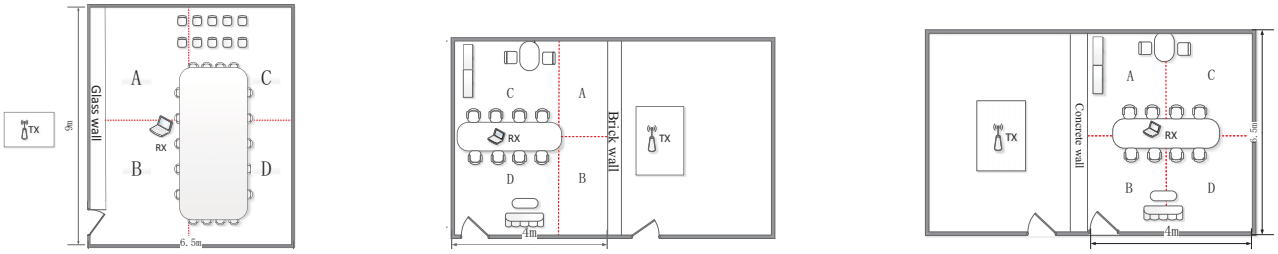

(a) Glass wall scene (b) Brick wall scene (c) Concrete wall scene

Fig. 6. Plan and division of different experimental scenes

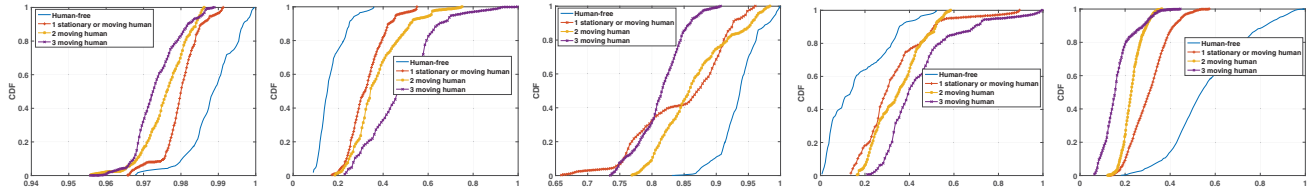

(a) Cumulative distribution function of λ_1 (b) Cumulative distribution function of λ_2 (c) Cumulative distribution function of γ_1 (d) Cumulative distribution function of γ_2 (e) Cumulative distribution function of ϕ_1

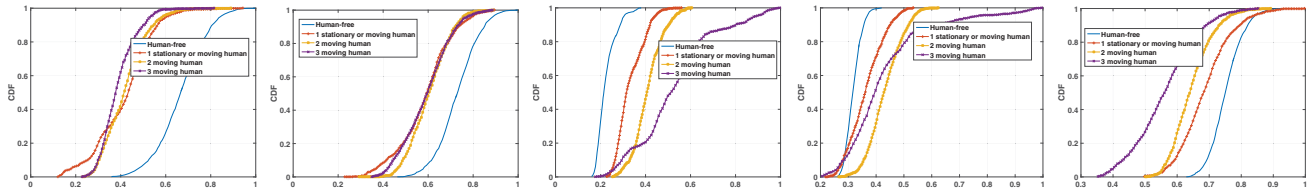

(f) Cumulative distribution function of ϕ_2 (g) Cumulative distribution function of ϕ_3 (h) Cumulative distribution function of β_1 (i) Cumulative distribution function of β_2 (j) Cumulative distribution function of β_3

Fig. 7. Cumulative distribution function of each signal feature in brick wall experimental scene

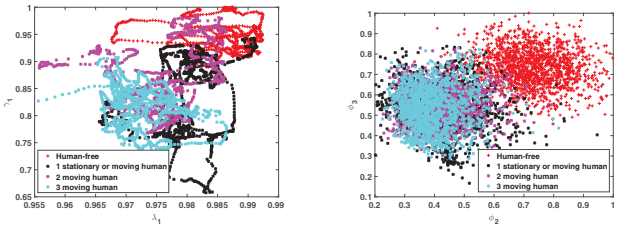

(a) DeMan (b) R-TTWD

Fig. 8. The detection results of DeMan and R-TTWD

accurately determined to the total number of samples in that category. We record the detection accuracy of no one, one moving human or one stationary human, two moving human, and three moving human as TR1, TR2, TR3, and TR4, respectively, and set the detection period to 1s, 2s, 3s, 4s, 5s, 6s, 7s, 8s, 9s, and 10s, respectively, the detection accuracy is shown in Fig.9. When the detection period is between 1s and 5s, the detection accuracy of each category is increases while the period greater than 5s, the detection accuracy tends to be stable. Therefore, the most appropriate period is 5s.

D. Comparison with other systems

In order to have a more objective assessment of TWMD, we compare it to the typical detection systems DeMan[10] and R-TTWD[14], as shown in Fig.10. The performance of DeMan is not well in all experimental scenarios, and the detection accuracy of each category is around 0.500. The assumption of DeMan[10] is that the useful signal is greater than the interference signal, but in the through-the-wall scenario, this condition is no longer satisfied, resulting in such poor detection accuracy. The performance of R-TTWD is well when detecting whether there exits humans. The TR1 values of the three experimental scenarios are 0.987, 0.926, and 0.886, respectively, but the performance is not satisfactory for detecting different numbers of moving human. By contrast, TWMD is superior to the above two systems in detection accuracy. In the glass wall scene, the accuracy of each category is 1.000, 0.993, 0.984 and 0.981, respectively. In the brick wall scene, the accuracy of each category is 1.000, 0.990, 0.907 and 0.939, respectively. In the concrete wall scene, the accuracy of each classification is 0.992, 0.939, 0.864 and 0.895, respectively. Through the analysis above, it can be considered that the multi-dimensional feature based detection algorithm proposed in this paper has a great performance improvement compared with the previous single feature-based detection algorithm, especially in the detection of the number of moving targets, the accuracy is improved by about 0.450. Furthermore, in the online detection phase, TWMD has no significant increase in time complexity compared with DeMan and R-TTWD. This is because the main calculations performed in TWMD are the same as them, that is, matrix decomposition.

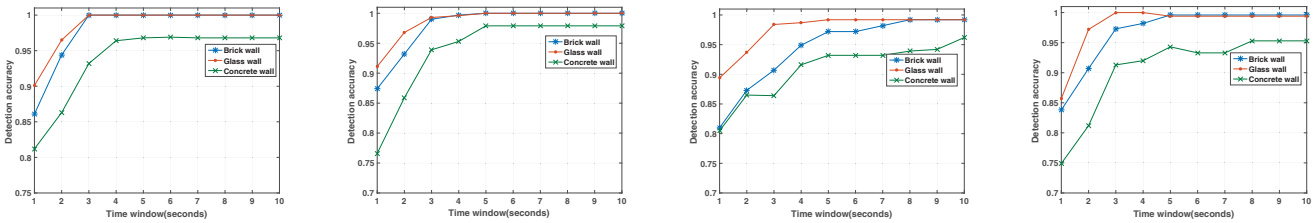

(a) TR1 (b) TR2 (c) TR3 (d) TR4

Fig. 9. Relationship between detection period and detection accuracy of each experimental scene

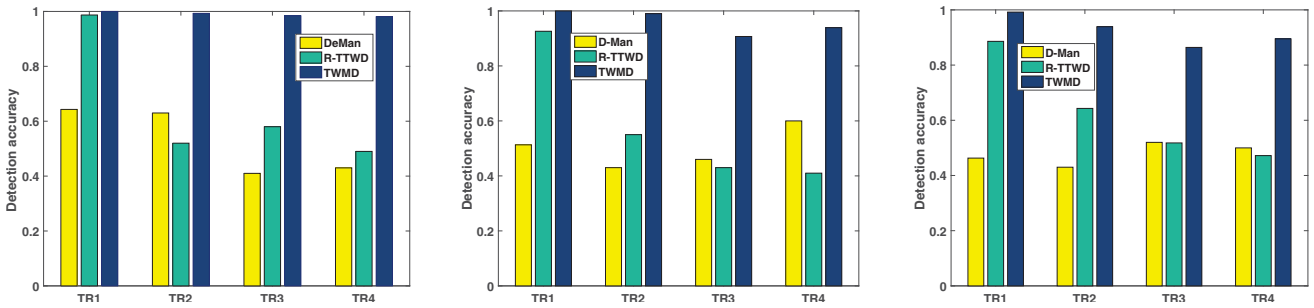

(a) Glass wall experiment scene (b) Brick wall experiment scene (c) Concrete wall experiment scene

Fig. 10. Comparison of detection accuracy between our system and other systems

V. Conclusion

In this paper, a human body target detection algorithm based on multi-dimensional signal features is proposed. Firstly, the received CSI is preprocessed to eliminate the phase error and the amplitude noise. Then, the multi-dimensional features are extracted by utilizing the time correlation and subcarrier correlation of CSI, and BP neural network is used to complete the mapping between features and categories. Experiment result shows that the recognition accuracy of our system in glass wall, brick wall and concrete wall environment are 0.980, 0.900 and 0.850 above, respectively. In future work, we will study through-the-wall detection when the transceiver is on the same side of wall. The difficulty is that the commercial WiFi signal bandwidth is small and the transceiver is not synchronized. Thus it is hard to suppress the direct wave and wall reflection signals. Our further research will seek a breakthrough from clutter suppression.

References

[1] F.Adib, H.Mao, and Z.Kabelac, “Smart homes that monitor breathing and heart rate,” in Proc. ACM Conference on Human Factors in Computing Systems, Seoul, 2015, pp.837-846.

[2] M.Jia, Z.Yin, D.Li, Q.Guo, and A.Gu, “Toward Improved Offloading Efficiency of Data Transmission in the IoT-Cloud by Leveraging Secure Truncating OFDM,” IEEE Internet of Things Journal, vol.6, no.3, pp.4251-4261, June 2019.

[3] M.Jia, Z.Yin, Q.Guo, G.Liu, and X.Gu, “Downlink Design for Spectrum Efficient IoT Network,” IEEE Internet of Things Journal, vol.5, no.5, pp.3397-3404, October 2018.

[4] M.Jia, X.Gu, Q.Guo, W.Xiang, and N.Zhang, “Broadband Hybrid Satellite-Terrestrial Communication Systems Based on Cognitive Radio toward 5G,” IEEE Wireless Communications, vol.23, no.6, pp.96-106, December 2016.

[5] M.Jia, Z.Gao, Q.Guo, Y.Lin, and X.Gu, “Broadband Hybrid Satellite-Terrestrial Communication Systems Based on Cognitive Radio toward 5G,” IEEE Transactions on Industrial Informatics, (Early Access), March 2019.

[6] A.Kosba, A.Saeed, and M.Youssef. “RASID: A robust WLAN device-free passive motion detection system,” 2012 IEEE International Conference on Pervasive Computing and Communications, Lugano, 2012, pp.180C189.

[7] J.Xiao, K.Wu, and Y.Yi, “FIMD: Fine-grained device-free motion detection,” in Proc. 2012 IEEE 18th International Conference on Parallel and Distributed Systems, Singapore, 2012, pp.229-235.

[8] W.Xi, J.Zhao, and X.Li, “Electronic frog eye: Counting crowd using WiFi,” in Proc.IEEE INFOCOM 2014 - IEEE Conference on Computer Communications, Toronto, 2014, pp.361-369.

[9] K.Qian, C.Wu, and Y.Zhang, ” PADS: Passive detection of moving targets with dynamic speed using PHY layer information,” in Proc. 2014 20th IEEE International Conference on Parallel and Distributed Systems (ICPADS), Hsinchu, 2014, pp.183-190.

[10] C.Wu, and X.Liu, “Non-Invasive Detection of Moving and Stationary Human With WiFi”, IEEE Journal on Selected Areas in Communications, vol.33, no.11, pp.2329-2342, May 2015.

[11] Z.Zhou, Z.Yang, and C.Wu, “Omnidirectional coverage for device-free passive human detection,” IEEE Transactions on Parallel and Distributed Systems, vol.25, no.7, pp.1819-1829, July 2015.

[12] F.Adib, and D.Kadabi, “See through walls with WiFi,” Acm Sigcomm Computer Communication Review,” Proceedings of the ACM SIGCOMM 2013 Conference on SIGCOMM, Hong Kong, 2013, pp.75-86.

[13] S.Domenico, M.Sanctis, E.Cianca,and M.Ruggieri, “Wi-Fi-based through-the-wall presence detection of stationary and moving humans analyzing the doppler spectrum,” IEEE Aerospace and Electronic Systems Magazine, vol.33, no.5, pp.14-19, May 2018.

[14] Z.Hai, X.Fu, L.Sun, R.Wang, and P.Yang, “R-TTWD: Robust device-free through-the-wall detection of moving human with WiFi,” IEEE Journal on Selected Areas in Communications, vol.35, no.5, pp.1090-1103, May 2017.

[15] F.Li, C.Xu, and Y.Liu, “Mo-sleep: Unobtrusive sleep and movement monitoring via Wi-Fi signal,” in Proc.2016 IEEE 35th International Performance Computing and Communications Conference (IPCCC), Las Vegas, 2016, pp.173-180.

[16] Tulsani.H, and Gupta.R, “1-D signal denoising using wavelets based optimization of polynomial threshold function,” in Proc.Proceedings of 3rd International Conference on Reliability, Infocom Technologies and Optimization, Noida, 2015, pp.126-131, January 2015.

[17] Y.Cun, B.Boser, and J.Denker,” Handwritten digit recognition with a back-propagation network,” Advances in Neural Information Processing Systems, vol.2, no.2, pp.396-404, May 1990.